IEEE Access
Multidisciplinary ⋮ Rapid Review ⋮ Open Access Journal

Received 9 July 2024, accepted 28 July 2024, date of publication 22 August 2024, date of current version 30 August 2024.

Digital Object Identifier 10.1109/ACCESS.2024.3439501

RESEARCH ARTICLE

Loss Minimization-Based Sensorless Control of High-Speed Induction Motor Considering Core Loss

TADELE AYANA, PIOTR KOŁODZIEJEK, MARCIN MORAWIEC, (Senior Member, IEEE), AND LELISA WOGI

Faculty of Electrical and Control Engineering, Gdańsk University of Technology, 80-233 Gdańsk, Poland

Corresponding author: Tadele Ayana (tadele.ayana@pg.edu.pl)

ABSTRACT This paper presents loss-minimizing sensorless control (LMC) strategies utilized to optimize the energy of high-speed induction motor (HSIM) drives. A machine's ability to operate effectively depends on the estimation of its electrical losses. Although copper losses account for the majority of electrical losses in electrical machines, core loss also contributes a major part, particularly in high-speed induction motors. A review of design solutions of power electronic converters to feed HSIMs and the effect of their parameters on iron losses were analyzed. In the gathered literature, HSIM loss analysis was generally performed using software analytical techniques such as finite element methods. There were few real-time loss analysis and loss minimization sensorless control approaches for HSIM in the literature. Finally, the study of sensorless control of 500Hz frequency with synchronous speed of 15000 rpm HSIM with optimal flux and reference reactive torque based optimization for loss minimization through nonlinear control system design was presented as a solution to the evaluated gaps found in the literature and the simulation findings were experimentally verified.

INDEX TERMS Sensorless control, loss minimization, energy optimal, high-speed induction motor.

I. INTRODUCTION

High-speed electric machines have gained popularity recently in many situations where it is preferable to do without the necessity of gearbox, lubrication-oil system, and other related accessory systems. Many benefits can be gained from increasing the speed of electric machines, such as decreased material consumption, decreased machine weight and size, decreased cost, increased dependability, reduced maintenance requirements and as well as their ability to adjust rotational speed across a broad range. High frequency motors find widespread usage in electric drives, including vacuum pumps, compressors, machine tools, woodworking gear, and even automobiles [1], [2], [3], [4], [5].

Sensorless speed control minimizes the trouble of re-entering the sensor in different applications, lowers costs, and prevents mechanical speed sensor fragility. Its application in industry is therefore expanding. Reliability of velocity data is essential for managing the speed of IM drives. It eliminates encoders or direct speed sensors are used to measure speed as they are more expensive, take up more room, require more wiring, require careful mounting, and feature electronics, among other drawbacks.

Field oriented control (FOC) at low speeds and voltage angle torque control (VATC) at higher speeds are combined which was developed for a high-speed sensorless IM drive. In the flux weakening domain, the voltage angle control method proposed here takes the position of flux-oriented control. Using the maximum amount of available inverter voltage, this strategy reduces the impact of estimated speed inaccuracy on the achieved flux level and addresses well-known problems associated with current control systems in settings where there is inadequate voltage margin [6].

The associate editor coordinating the review of this manuscript and approving it for publication was Qinfen Lu.

Efficiency increases are correlated with faster motor speeds. Thus, an important issue is maintaining effective machine control at high speeds. A review of the literature helps determine the optimal control strategy. It seems that the other benefit is the most crucial. By matching each tool's speed with the output frequency of the inverter, a single drive may run numerous tools. Slowing down the machine when it's not in use also contributes to energy conservation and noise reduction. A tool can be swiftly updated if it is in great demand. There is a comparison between two types of high-speed drives [7], one having a gearbox and the other a frequency converter.

The literature on high-speed electric machines lacks detailed analysis of core loss which is one of the challenge in HSIM design. Inductors and transformers used in high frequency dc/dc converters require core loss estimation under arbitrary stimulation. There is limited study on designing high-speed electric machines and estimating core loss at high fundamental frequencies.

As the frequency of operation increases, core loss in electric machines becomes more significant, emphasizing the need of estimating core loss. Estimating the core of electric machines at high frequencies is hard due to factors including magnetic flux density, harmonics, and machine dimensions [8].

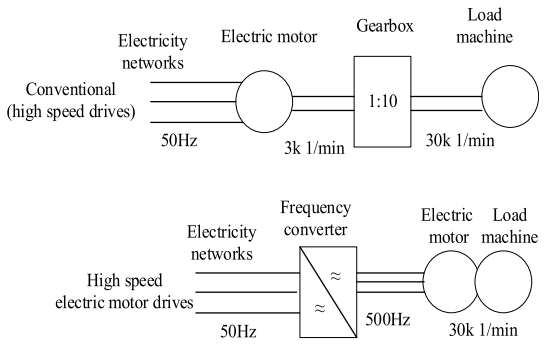

FIGURE 1. Difference between drives using either a gearbox or an inverter fed high-speed electric motor [9].

II. LOSSES AND LOSS MINIMIZATION IN HSIM's

High-speed induction motors differ from classical IMs with a frequency supply of 50 Hz due to their higher frequency and distinct loss distribution.

Distribution of loss in an electrical motor consist of three parts [10];

$$P_L = p_{cu} + p_{fe} + p_f \tag{1}$$

where P_L total power loss, p_{cu} is the sum of stator (p_{sCu}) and rotor (p_{rCu}) copper losses, p_{fe} core losses and p_f friction losses.

For constant current density, p_{cu} is proportional to the volume of winding copper and it is independent of speed.

p_{fe} has two parts: hysteresis loss (p_h) and eddy current loss (p_e). The hysteresis loss is proportional to the frequency, or speed (n), while the eddy current loss is proportional to the frequency squared.

$$p_{fe} = p_h + p_e \tag{2}$$

$$p_h = k_h n$$

$$p_e = k_e n^2 \tag{3}$$

The proportionality factors, k_h and k_e are proportionate to the motor's volume, assuming constant flux density in iron as speed changes.

The friction loss p_f is related to the cube of the speed.

$$p_f = k_f n^3 \tag{4}$$

The proportionality factor k_f is proportionate to the motor volume.

Electric motors' output power is proportional to their rotor volume and speed.

$$p_{out} = \gamma v_r n = \delta n \tag{5}$$

where γ is the utilization factor, v_r is the rotor volume, and $\delta = \gamma v_r n$ constant.

The motor's efficiency is expressed by,

$$\eta = \frac{P_L}{P_{out}} \tag{6}$$

As p_{cu}, p_h, p_e, p_f, and δ are proportional to the motor volume, it is possible to draw the following conclusions for HSIMs as in table 1 below.

TABLE 1. The relationship between loss distributions and speed of HSIM.

Loss components	Relation with speed (n)
Copper loss (p_{cu})	decreases with increasing n
Hysteresis loss (p_h)	remains constant
Eddy current loss (p_e)	increases proportionally
Friction loss (p_f)	increases with the square of n

To conform the conclusion in table 1 above drawn from mathematical expressions (1)-(6), the loss distribution of a conventional 37 kW 1500-rpm versus a 37 kW 50000-rpm HSIMs is presented in fig 2 below [11].

III. HSIM CONTROL TECHNIQUES AND CHALLENGES

High-speed drives are still being investigated, but reports concerning this topic are currently limited in the literature.

The description provided at the outset clearly demonstrates the benefits of HSIM drives. It determines the importance of developing stable and efficient control. Most proposed algorithms rely on vector control. Direct torque control (DTC) is a popular control system for low to medium speed applications. It ensures that torque and flux are controlled instantly. However, achieving DTC might be challenging at high speeds. The fundamental reason for this is the difficulty in obtaining high sampling rates in high velocity ranges. References show that FOC strategies for high-speed applications produce excellent

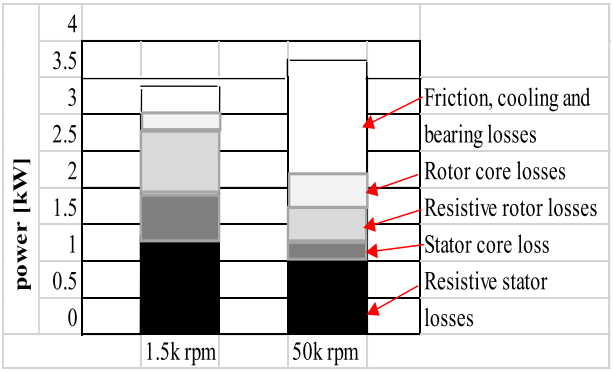

FIGURE 2. Power losses of a standard 37 kW and HSIM [11] (edited).

outcomes when compared to scalar and DTC. The majority of reports show application of sensorless control, with only one using a high-performance speed sensor. Significant issue with these kind of applications is determining optimum speed and position [12].

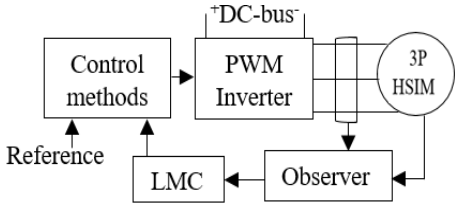

FIGURE 3. Block diagram of sensorless HSIM drive control under loss minimizing control (LMC).

Review of solutions used in the overall closed loop performance presented by each components of block diagram in figure 3, presented as follows;

A. CONTROL METHODS USED TO DATE IN HSIM

There is limited information concerning explicit identification of controllers or advanced control solutions applied for strongly nonlinear systems in the literature. Complexity of the control algorithm is one of the most important challenges associated with HSIMs.

B. PWM INVERTERS IN HSIM

Advancements in semiconductor power electronics enable high-power inverters with compact dimensions and high output voltage frequencies. High switching frequencies and high power levels in modern semiconductor devices can cause large commutation losses. Inverters with half-cycle switching, along with a regulated DC/DC converter, are utilized to feed the motor, in addition to PWM inverters that provide a favorable voltage waveform to the receiver.

Using proper topologies and inverter control approaches, receiver current waveforms can be generated with minimal switching. Adding LC filters between the inverter and receiver can reduce distortion in voltage and current waveforms, but increases the solution's weight and cost.

The effects of the following inverter parameters are taken into account in [13], [14], [15], and [16], modulation index, waveform, and switching frequency and the following recommendations were pointed out.

Motor iron losses are significantly influenced by the modulation index. Therefore, it is preferable to operate with the maximum permitted modulation index in order to minimize iron losses. Use of inverters with fixed and high modulation index and changing dc bus voltage can be thought of as a good solution, especially for applications where the energetic performances are significant in comparison to the dynamic ones.

From the perspective of iron losses, the switching frequency is not very significant. One can achieve a slight decrease in core losses, specifically as the switching frequency increases. Naturally, in order to accurately assess the efficiency of the system (motor and inverter) as the switching frequency is increased, it is crucial to account for the loss increase within the power switches.

The waveform of the modulation function has no significant impact on the rise in iron losses. In actuality, the motor iron losses remain unchanged by the three commonly used modulation waveforms (sinusoidal, sinusoidal plus third harmonic, and space vector). Induction motors powered by PWM inverters have higher iron losses than those determined by sinusoidal supplies [17], [18], [19].

C. DESIGN CONSIDERATION OF HSIM

HSIMs are almost as efficient as low-speed motors (up to 377 rad/s). However, the loss distribution of HSIM can differ based on design factors.

There have been some concerns about this. Higher-speed motors have a smaller cooling surface. It indicates that the motors' power losses are equivalent. This causes problems with the cooling system.

The HSIM stator is identical to a regular motor, however the key issue is minimizing power losses.

In addition, thick lamination is used. The rotor is the most significant component of the HSIM.

A HSIM's mechanical performance is dictated by the mechanical stress imposed by centrifugal force on the laminations and squirrel cage. Rotor balancing is essential for long-life bearings. Proper air gap construction is critical for air change and hit dissipation, as friction losses are significant.

Experimental research on high-speed solid and composite rotor induction motors, high-speed induction motors with changing rotor core architecture, thermal simulation of a high-speed solid-rotor induction motor, high-speed electric machinery: difficulties and design issues, and high-speed motor performance evaluation for electric vehicles [20], [21], [22], [23], but no control mechanism and observer structure is considered.

A technique for analyzing solid-rotor induction motors operating at high speeds is demonstrated. The study is based on a novel fusion of the transfer-matrix approach and the

three-dimensional linear method. The implications of finite length and saturation are considered. For dynamic thrust compensation, a vector control technique is put forth for the real-time change of torque current and slip-frequency. A semi-analytical approach for computing the eddy current losses in the solid rotor of a high speed squirrel cage induction motor, making structural modifications to the stator to get rid of significant effective space harmonics, an inventive design is put forth that represents a novel stator and rotor combination that is not obtained in prior studies with potential gains in both theory and practical application for a high-speed solid-rotor induction machine's efficiency has been analysed in [24], [25], and [26].

D. ESTIMATOR/SENSORLESS CONTROL

The necessity of using estimator for parameters identification is more challenging in HSIM than the conventional induction motors as it will be difficult to use or mount encoder or other meters for high speed rotating machines. Mechanical sensors positioned in shafts are often unreliable due to electromagnetic (EMI) interference. Due to their high spinning speed, (angle information given by Hall-effect sensors offer unreliable measurements with a resolution of only $\pm 30^{o}$) [27]. Moreover due to their construction rules encoders designed for high speed range show low accuracy at lower speeds.

The IM mathematical model serves as the foundation for the most common speed observer structure techniques. Algorithmic techniques include the Kalman filter [28], sliding technique structures [29], and backstepping structures [30], adaptive full-order (AFO) observer [31]. They also offer a mix of complete and reduced-order state observers, nonadaptive rotor speed estimation for an induction machine using an adaptive full-order observer, the model reference adaptive system are typical type of feedback utilized by closed-loop observers in sensorless control of conventional induction motor. But in the collected literatures none of these has been applied for HSIM so far.

E. LOSS MINIMIZING CONTROLS (LMC)

The techniques can be divided into two categories: Online search power controllers assess input power and continuously adjust the flux level until they locate the lowest amount of input power. Although they are unaffected by the motor's specifications, they frequently converge slowly, potentially resulting in torque and flux pulsations. Loss-model-based controllers (LMCs) use functional loss models to determine the ideal flux rate.

In [32] and [33], sensorless HSIM control is preformed, either loss analysis or loss minimization control is not considered in these papers.

It is rare to find sensorless speed control of HSIM incorporating loss minimizing controls (LMC) in the literatures up to date whereas only some loss analysis has been done [2], [8]. Different classical control approaches without observer and detail analysis of losses were presented in [34], [35], and [36] with no stability analysis.

Fig 4 below shows possible loss minimizing control algorithms to be implemented for HSIM based on applications.

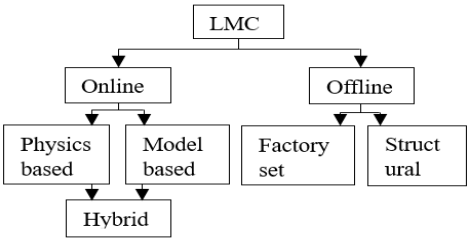

FIGURE 4. Types of LMC's.

Following the above-mentioned literature evaluations, the following research gaps have been identified.

1. From the loss minimizing control view using optimum flux in control strategies that have too much effect on the drives' steady-state performance is what the examined literature mostly has in common when it comes to nonlinear control. But in the process, the algorithm's computational performance is mostly impacted. As a result, higher computational load is anticipated in exchange for improved steady-state performance. Still, the driving dynamics are typically the primary emphasis of a closed-loop control strategy. Most of the literature find no trade-off between the computing maximum torque and reactive torque.
2. There were less stability analysis of observer and PI controllers tuning gains selection which needs more attention to be given.
3. In loss minimizing control usually used in most of the literatures were applicable during steady state operation as the motor can sustain its natural internal stabilization, but it will not give satisfactory loss analysis during dynamic state.
4. During sensorless control system design selection of tuning gains in the observer structure will affect the overall system performance.

In order to fill in the aforementioned research gaps, the current work suggests an IM drive optimum reactive torque reference generation method.

1. A review of the impact of inverter parameters on iron losses in induction motors fed by PWM inverters in different literatures was presented.
2. Optimum loss control based on generating reference reactive torque was proposed
3. The comparison of proposed optimization with the widely used optimum flux used in most of the literatures was presented showing more robustness specially in dynamic state reducing the loss components more.
4. Reduction of PI controllers and hence less tunings
5. Stability analysis of speed observer structure and selection of PI controller gains were analysed in detail.

6. An updated machine model was used by considering core loss through equivalent core loss resistance both in the control method and observer structure.

IV. PROPOSED SOLUTIONS

In this section the sensorless control of HSIM by incorporating all the necessary components in the closed loop system with LMC was conducted both by simulation and experimental results.

A. INDUCTION MOTOR MODEL

In the stationary reference frame, the vector model of the HSIM can be represented as conventional induction motor differential equations for the stator current vector and the rotor flux vector of the following form as [31]:

$$\frac{di_{s\alpha}}{dt} = a_1 i_{s\alpha} + a_2\phi_{r\alpha} + a_3\omega_r\phi_{r\beta} + a_4 u_{s\alpha}$$
$$\frac{di_{s\beta}}{dt} = a_1 i_{s\beta} + a_2\phi_{r\beta} - a_3\omega_r\phi_{r\alpha} + a_4 u_{s\beta} \quad (7)$$
$$\frac{d\phi_{r\alpha}}{dt} = a_5\phi_{r\alpha} - \omega_r\phi_{r\beta} + a_6 i_{s\alpha}$$
$$\frac{d\phi_{r\beta}}{dt} = a_5\phi_{r\beta} + \omega_r\phi_{r\alpha} + a_6 i_{s\beta} \quad (8)$$
$$\frac{d\omega_r}{dt} = \frac{L_m}{JL_r}(\phi_{r\alpha} i_{s\beta} - \phi_{r\beta} i_{s\alpha}) - \frac{T_L}{J} \quad (9)$$

where the following coefficient designations have

$$a_0 = \frac{L_r L_s - L_m^2}{L_r L_s},\ a_1 = \frac{-(R_s + R_c)L_m^2 R_r + R_s R_c L_r^2}{a_0 L_s (R_s + R_c) L_r^2},$$
$$a_2 = \frac{L_m R_r}{a_0 L_s L_r^2},\ a_3 = \frac{L_m}{a_0 L_s L_r},\ a_4 = \frac{R_c}{a_0 L_s (R_c + R_s)},$$
$$a_5 = \frac{-R_r}{L_r},\ a_6 = -a5 L_m,\ a_{12} = 1 + a_9 - a_{10}^2,$$
$$a_{13} = a_7 - a_{11}^2,\ a_{14} = -(a_8 + 2a_{10}a_{11})\ a_7 = \frac{1}{L_r^2},$$
$$a_8 = \frac{2Lm}{L_r^2}, a_9 = \frac{L_m^2}{L_r^2},\ a_{10} = \frac{L_s L_r - L_m^2}{L_r^2 L_m},\ a_{11} = a_7 Lr$$

where T_L is load torque, J is the rotor moment of inertia, $u_{s\alpha}$, $u_{s\beta}$ are the stator voltages, $i_{s\alpha}$, $i_{s\beta}$ are the stator currents, $\phi_{r\alpha}$, $\phi_{r\beta}$ are the rotor fluxes, and ω_r is the rotor velocity, and moreover, R_s is stator, R_r is rotor, R_c is core resistances and L_s is stator, L_r is rotor, L_m is mutual inductance. It should be emphasized that all variables and parameters discussed in the study are expressed in the p.u. system.

B. PROPOSED CONTROL SYSTEM

The multiscalar model is an induction-machine model with scalars and coordinate system independent state variables that was initially introduced in [37].

Now, the selected state variables are the following general form of equations.

$$w = [i_{s\alpha}\ i_{s\beta}\ \phi_{r\alpha}\ \phi_{r\beta}\ \omega_r]^T \quad (10)$$

and the derivative of (10) is;

$$\dot{w} = [\dot{i}_{s\alpha}\ \dot{i}_{s\beta}\ \dot{\phi}_{r\alpha}\ \dot{\phi}_{r\beta}\ \dot{\omega}_r]^T \quad (11)$$

The multiscalar variables transformation can be expressed as,

$$w_{11} = \omega_r$$
$$w_{12} = \phi_{r\alpha} i_{s\beta} - \phi_{r\beta} i_{s\alpha}$$
$$w_{21} = \phi_{r\alpha}^2 + \phi_{r\beta}^2$$
$$w_{22} = \phi_{r\alpha} i_{s\alpha} + \phi_{r\beta} i_{s\beta} \quad (12)$$

where the variable w_{11} is rotor speed, w_{12} is proportional to electromagnetic torque, w_{21} is the square of the rotor flux, and w_{22} is energy proportional.

The differential equation that represents the changed variables in (12) is written as follows.

$$\frac{dw_{11}}{dt} = \frac{L_m}{JL_r} w_{12} - \frac{m_o}{J} \quad (13)$$
$$\frac{dw_{12}}{dt} = T_m w_{12} + m_1 \quad (14)$$
$$\frac{dw_{21}}{dt} = -2a_5 w_{21} + 2a_6 w_{22} \quad (15)$$
$$\frac{dw_{22}}{dt} = -T_m w_{22} + m_2 \quad (16)$$

where T_m is the motor electromagnetic time constant, m_o is load moment, J is inertia, u_1 and u_2 are control variables included in m_1 and m_2 respectively. moreover, they can be expressed as;

$$T_m = \frac{R_r}{(L_r - L_{\boldsymbol{m}})}$$
$$u_1 = \phi_{r\alpha} u_{s\beta} - \phi_{r\beta} u_{s\alpha}$$
$$u_2 = \phi_{r\alpha} u_{s\alpha} + \phi_{r\beta} u_{s\beta} \quad (17)$$

The PI controller of the state variables w_{12} and w_{22} generates the control signals m_1 and m_2 correspondingly.

$$u_1 = \frac{1}{a_4}(w_{11}(w_{22} + a_3 w_{21}) + m_1)$$
$$u_2 = \frac{1}{a_4}(-w_{11} w_{12} - a_2 w_{21} - a_6(i_{sx}^2 + i_{sy}^2) + m_2) \quad (18)$$

The needed voltage components for the PWM algorithm ($u_{s\alpha}$ and $u_{s\beta}$) are as follows:

$$u_{s\alpha} = \frac{\phi_{r\alpha} u_2 - \phi_{r\beta} u_1}{w_{21}}$$
$$u_{s\beta} = \frac{\phi_{r\alpha} u_1 + \phi_{r\beta} u_2}{w_{21}} \quad (19)$$

C. LOSS MINIMIZATION TECHNIQUES

Proposal 1 (Optimum Flux for Loss Minimization): The adjustable-speed controller in high-performance drives is primarily responsible for tracking the reference speed as rapidly as feasible. On the one hand, it is commonly known, as stated in the following chapter, that induction motors should be run at a lower flux during light loads to save energy.

The problem with light load operation, on the other hand, is determining how to respond as quickly as feasible during a major load shift [38]. As a result, when the step speed command increases at low load and flux levels, the nominal growth reference value could be used for system boundaries.

Now the loss equation in can be re-written as;

$$P_L = 1.5(R_s I_s^2 + R_r I_r^2 + R_c I_{Rc}^2) \tag{20}$$

where I_s^2, I_r^2, I_{Rc}^2 are stator, rotor, core currents magnitudes respectively.

P_L can be regarded of as a cost function because it is a positive definite function that can be decreased by any desired variables.

Because the purpose of this review is to create the optimum value of flux using a multiscalar variable that delivers the lowest possible loss of an HSIM and maximizes power efficiency, air gap fluxes were chosen as the desired variables to lower the power loss cost function.

The iron loss ($R_c I_{Rc}^2$) in (20) can also be rewritten as;

$$p_{fe} = k_h \omega w_{21} + k_e \omega^2 w_{21} \tag{21}$$

where ω is the stator angular frequency, k_e and k_h are the eddy-current and hysteresis loss coefficients.

In a high-frequency zone, the eddy current loss is greater than the hysteresis loss. As a result, the stator $p_{fe}(s)$ and rotor $p_{fe}(r)$ iron losses are approximated as follows:

$$p_{fe}(s) = (k_e \omega^2 + k_h \omega) w_{21} \approx \left(\frac{\omega^2 w_{21}}{1/k_e}\right) \tag{22}$$

$$p_{fe}(r) = (k_e s^2 \omega^2 + k_h s \omega) w_{21} \approx \left(\frac{s^2 \omega^2 w_{21}}{1/k_e}\right) \tag{23}$$

where s is motor slip and since $|s\omega| \ll |\omega|$ rotor iron loss may be omitted.

Expressing rotor currents interms of multiscalar variables from (24) obtained as (25),

$$\begin{aligned} L_r i_{r\alpha} &= \phi_{r\alpha} - L_m i_{s\alpha} \\ L_r i_{r\beta} &= \phi_{r\beta} - L_m i_{s\beta} \end{aligned} \tag{24}$$

$$i_r^2 = a_7 w_{21} - a_8 w_{22} + a_9 i_s^2 \tag{25}$$

Now the total power loss (P_L) can be written as:

$$P_L = \rho_1 \frac{w_{12}^2}{w_{21}} + \rho_2 w_{21} \tag{26}$$

where;

$$\begin{aligned} \rho_1 &= (R_s L_r^2 + R_r L_m^2)/L_r^2 \\ \rho_2 &= (R_s/L_m^2) + (\omega^2/R_c) \end{aligned} \tag{27}$$

When the multiscalar variable w_{21} is at steady state, the loss minimization condition is given by;

$$\frac{\partial P_L}{\partial w_{21}} = 0 \tag{28}$$

The solution to the differential equation (28) is,

$$w_{21*(\text{optimum})} = \sqrt{\frac{\rho_1}{\rho_2}}\,|w_{12}| \tag{29}$$

where ρ_1 and ρ_2 are both calculated to be positive real numbers.

Proposal 2 (Reactive Torque Based Optimization): Generating reference reactive torque based optimization for loss minimum control to improve variable flux operation is proposed by maximum electromagnetic torque per reactive torque principle where variable flux operation is used for example in electric vehicle applications.

The control technique for an induction motor that maximizes torque response and efficiency in both transient and steady state conditions is presented in this study. The optimum issue in the context of vector control of an induction motor is formulated using the calculus of variations for a specific step change of the reference torque.

The problem can be viewed as a conventional calculus of variations problem since a suitable mathematical definition of the problem entails finding a function that minimizes a given functional, as demonstrated in [38] and [39]. Though the latter only provided an approximate answer and assumed a constant speed during torque transients, the former produced neither simulation nor experimental results.

The use of the variational approach to obtain the closed-form analytical solution of the problem of determining the time trajectories of the reference reactive torque components in the vector control of an induction motor that minimize the stator current amplitude for a given step variation of the reference torque defines the contribution of this paper. The suggested control technique is both viable and valid, as confirmed by simulation and experimental findings.

Finding a feedback control that satisfies torque tracking control objectives while minimizing a generalized convex energy cost function that includes the stored magnetic energy and coil losses is the issue to be taken into consideration.

The physical meaning of reactive torque (w_{22}) is somehow proportionate to the energy and also called magnetized variable, which is connected to the concept of control explained in detail. It is referred to as the reactive torque or magnetizing variable since it is orthogonal to w_{12} and shares the same dimensions and time scale. As reactive torque is related to the magnetizing state of the machine reducing the magnetizing state of the machine can be regarded as one way of core loss minimization technique.

From the general equation;

$$\begin{aligned} i_{m\alpha} &= i_{s\alpha} + i_{r\alpha} \\ i_{m\beta} &= i_{s\beta} + i_{r\beta} \end{aligned} \tag{30}$$

where $i_{m\alpha}$ and $i_{m\beta}$ are the $\alpha - \beta$ components of the magnetizing currents.

Solving for magnetizing currents

$$\begin{aligned} i_{m\alpha} &= \frac{((L_s L_r - L_m^2) - (L_s - L_m) L_r) i_{s\alpha}}{L_r^2 L_m} + \frac{\phi_{r\alpha}}{L_r} \\ i_{m\beta} &= \frac{((L_s L_r - L_m^2) - (L_s - L_m) L_r) i_{s\beta}}{L_r^2 L_m} + \frac{\phi_{r\beta}}{L_r} \end{aligned} \tag{31}$$

$$i_m^2 = a_{10}^2\left(\frac{w_{12}^2 + w_{22}^2}{w_{21}}\right) + a_{11}^2 w_{21} + 2a_{10}a_{11}w_{22} \tag{32}$$

Now (30) can be written as,

$$a_{12}w_{12}^2 + a_{12}w_{22}^2 + a_{13}w_{21}^2 + a_{14}w_{22}w_{21} = 0 \tag{33}$$

Solving for electromagnetic torque,

$$w_{12} = \sqrt{-w_{22}^2 - \frac{a_{13}}{a_{12}}w_{21}^2 - \frac{a_{14}}{a_{12}}w_{22}w_{21}} \tag{34}$$

Remark: Using maximum electromagnetic torque per reactive torque;

$$\frac{\partial w_{12}}{\partial w_{22}} = 0.5\frac{(-2w_{22} - \frac{a_{14}}{a_{12}}w_{21})}{\sqrt{-w_{22}^2 - \frac{a_{13}}{a_{12}}w_{21}^2 - \frac{a_{14}}{a_{12}}w_{22}w_{21}}} = k_1 \tag{35}$$

Solving for reactive torque from (35),

$$w_{22*(\text{optimum})} = \frac{-a_{16} \pm \sqrt{a_{16}^2 - 4a_{15}a_{17}}}{2a_{15}}$$
$$a_{15} = 1 + k_1^2, \quad a_{16} = \frac{a_{14}}{a_{12}}(k_1^2 - 1)w_{21}, \tag{36}$$

where,

$$a_{17} = (0.25\frac{a_{14}}{a_{12}} + k_1^2\frac{a_{13}}{a_{12}})w_{21}^2$$

and k_1 can be constant carefully selected to get required flux level or solved by setting (35) to zero for $w_{22} = 0$.

This solution is the optimum reference reactive torque used to control flux without using flux controller in the control system structure.

To account for changeable command flux in the vector controlled induction machine, iron loss resistance must be described as a function of frequency and flux dependent parameters in the control system which is usually not emphasized and presented in the literatures so far specially for HSIM. It can be stated empirically as [40]:

$$R_c = R_{cm}\left(\frac{f}{f_{rated}}\right)^{1.1}\left(\frac{\phi}{\phi_{rated}}\right)^2 \tag{37}$$

where R_{cm} core or iron loss resistance is measured from the standard no-load test, f_{rated} and ϕ_{rated} values are at the designated frequency and flux, respectively. The model with constant R_{cm} yields unacceptable results because changes in frequency and flux should cause the magnetizing resistance R_{cm} to vary.

D. OBSERVER DESIGN

Achieving high performance sensorless control of HSIM requires precise flux estimation. The concept for the AFO speed observer design process was presented in [31].

$$\frac{d\hat{i}_{s\alpha}}{dt} = a_1\hat{i}_{s\alpha} + a_2\hat{\phi}_{r\alpha} + a_3\hat{\omega}_r\hat{\phi}_{r\alpha} + a_4u_{s\alpha} + \Delta i_1 + z_\alpha$$
$$\frac{d\hat{i}_{s\beta}}{dt} = a_1\hat{i}_{s\beta} + a_2\hat{\phi}_{r\beta} - a_3\hat{\omega}_r\hat{\phi}_{r\beta} + a_4u_{s\beta} + \Delta i_1 + z_\beta \tag{38}$$

$$\frac{d\hat{\phi}_{r\alpha}}{dt} = a_5\hat{\phi}_{r\alpha} + a_6\hat{i}_{s\alpha} - \hat{\omega}_r\hat{\phi}_{r\beta} + z_{\phi\alpha}$$
$$\frac{d\hat{\phi}_{r\beta}}{dt} = a_5\hat{\phi}_{r\beta} + a_6\hat{i}_{s\beta} - \hat{\omega}_r\hat{\phi}_{r\alpha} + z_{\phi\beta} \tag{39}$$

where estimated values are denoted by "^", and stabilizing functions $z_{\alpha,\beta}$ and $z_{\phi\alpha,\beta}$ are included in the structure. Only the stator current derivatives are updated using the bounded parametric uncertain terms.

$$z_\alpha = -(\lambda_a + \Delta i_1)e_{is\alpha}$$
$$z_\beta = -(\lambda_a + \Delta i_2)e_{is\beta} \tag{40}$$

where $e_{is\alpha}, e_{is\beta}$, are stator $\alpha - \beta$ component current errors between their actual and estimated values. The flux component stabilizing functions are;

$$z_{\phi\alpha} = -\gamma_1 e_{is\alpha} + \gamma_2\hat{\omega}_r e_{is\beta}$$
$$z_{\phi\alpha} = -\gamma_1 e_{is\beta} - \gamma_2\hat{\omega}_r e_{is\alpha} \tag{41}$$

where λ_a, γ_1, γ_2 are observer tuning gains (feedback gains) which are in (38)–(39) are chosen by pole placement method of linearized observer structure which is discussed in detail under stability analysis section.

The integrator can be used to replicate the value of rotor speed from an adaptive mechanism [31] as,

$$\frac{d\hat{\omega}_r}{d\tau} = \xi a_3(\hat{\phi}_{r\alpha}(i_{s\beta} - \hat{i}_{s\beta}) - \hat{\phi}_{r\beta}(i_{s\alpha} - \hat{i}_{s\alpha})) \tag{42}$$

where $\xi = 0.9$ is adaptation tuning gain.

V. ANALYSIS AND RESULTS

A. STABILITY ANALYSIS

Other stability analyses of the speed estimate in the AFO structure were reported in [31] and [41], which addressed some of the flaws of [42] and highlighted how different tuning gains affect the linearized observer system's stable working range when extra feedback is available. The tuning increases are chosen arbitrarily to show how the value of various gains affects observer pole location. However, none of them account for the influence of iron or core loss resistance in their mathematical models of the IM and AFO observer structures, whereas the control system proposed in this study is unique in that it avoids nonlinearity.

To stabilize the system, the coefficients $\lambda\alpha$ and ξ were introduced. A linearized system generally has the following form:

$$\frac{d}{dt}\Delta\mathbf{x}(t) = \mathbf{A}\Delta\mathbf{x}(t) + \mathbf{B}\Delta\mathbf{u}(t) \tag{43}$$

where A and B are the state space representation's Jacobian matrices, and $\Delta\mathbf{x}(t)$ is the estimation error of stator currents, magnetizing fluxes, and speed, and $\Delta\mathbf{u}(t)$ is considered as known control input.

The solution to (43) is given by;

$$\Delta\tilde{\mathbf{i}}_s = [s\mathbf{I} - \mathbf{A}]^{-1}\Delta\mathbf{A}\hat{\mathbf{x}} \tag{44}$$

In some circumstances, the eigenvalues of the matrix are evaluated at different operational points.

Case 1) $\omega r = 1$, $\lambda\alpha = 2$, $\gamma_1 = 0.2 \ldots 4$, $\xi = 0.2$, $\gamma_2 = 3$ (these parameters are contained in matrix A).

The spectrum of the matrix for the linearized observer system is shown by figure 5 as ξ coefficient is varied from 0.2…4 for the nominal value of the load torque and rotor speed. The observer system is stable for ξ greater than zero and various modifications of other gains $\lambda\alpha$ and (ξ, γ_2).

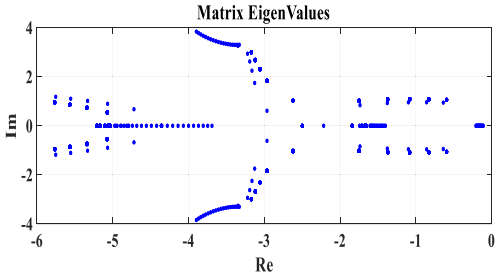

FIGURE 5. Spectrum of matrix of the linearized AFO observer system.

Case 2) $\omega_r = -1..1$, $\lambda\alpha = 0.6$, $\gamma_1 = 0.7$, $\xi = 0.6$, $\gamma_2 = 0.7$

The spectrum of the linearized observer's matrix is shown in figure 6 for $\lambda\alpha = 0.6$ when the rotor speed changes from -1.0 to 1.0 p.u. and TL = 0.7 p.u. The poles of the observer structure are all negative values and stable.

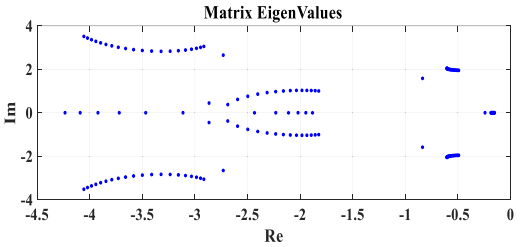

FIGURE 6. Spectrum of matrix of the linearized observer system.

B. SELECTION OF PI CONTROLLERS GAINS

Four PI controllers are shown in the control diagram in Figure 24, two for regulating speed and flux and two for regulating electromagnetic and reactive torques. Their main goal is to ensure the drive stability and proper operation. To achieve these their parameters must be chosen correctly to control the drive system. One way to choose these gains is using stability boundary locator (SBL) method, finds the controller settings that stabilize a closed-loop system analysis using a graphical approach and depends on the controller parameters (k_p, k_i) and frequency (ω). The feedback control system that is used should be able to achieve the following design objectives: reduced susceptibility to noise in measurements, stability in closed loops, appropriate rejection of disturbances, fast tracking of set points, and an appropriate degree of resilience to process changes and ambiguity in the model.

Figure 7 uses cascade PI controllers for reactive torque and flux loops (b) and electromagnetic torque and speed control loops (a).

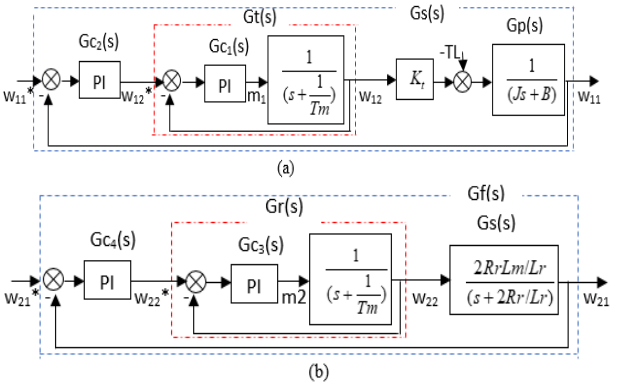

FIGURE 7. (a) Cascade PI controllers for electromagnetic torque and speed control loops, (b) reactive torque and flux.

The electromagnetic torque loop can be expressed analytically as,

$$G_t(s) = \frac{G_{c1}(s)T_m}{sT_m + G_{c1}(s)T_m} \approx \frac{\omega_n^2}{s^2 + 2\zeta\omega_n s + \omega_n^2} \tag{45}$$

As shown in (45), where ω_n is the natural frequency and ζ is damping ratio, the closed-loop system is second-order matched to the conventional canonical form.

With design specifications taken as, maximum overshoot of 2% or less, 2% settling in less than a second (t_s), and a peak duration of less than 0.50 seconds (t_p).

$$\delta \cong \frac{4}{t_s}, \quad \vartheta \cong \frac{\pi}{t_p} \tag{46}$$

where (δ, ϑ) are optimal closed-loop pole placements and positions.

The maximum percent overshoot criterion is,

$$M_p = e^{-\zeta\pi/\sqrt{1-\zeta^2}} \tag{47}$$

Choosing $\zeta = 0.707$,

$$\omega_n = \frac{\delta}{2\zeta} = 5 \tag{48}$$

$k_{i12} = \omega_n^2 = 25$ and $0.775 + k_{p12} = 2\zeta\omega_n \Rightarrow k_{p12} = 6.225$

For speed loop, let $G_{01}(s)$ open loop TF and $\Delta C_1(s)$ is closed-loop characteristic equation excluding $G_{c1}(s)$,

Using $G_{01}(s)$ for speed open loop TF and $\Delta C_1(s)$ the closed-loop characteristic equation, excluding $G_{c2}(s)$,

$$G_{o1}(s) = G_t(s)K_tG_p(s) = \frac{6.074s + 24.39}{0.045s^3 + 0.355s^2 + 1.405s + 1} \tag{49}$$

The open loop $G_{o1}(s)$ can also be written as splitting its numerator and denominator equations into even and odd functions and substituting $(s = j\omega)$ [43],

$$G_{o1}(j\omega) = \frac{N(j\omega)}{D(j\omega)} = \frac{N_e(-\omega^2) + j\omega N_o(-\omega^2)}{D_e(-\omega^2) + j\omega D_o(-\omega^2)} \tag{50}$$

The system characteristic's equation can be written as,

$$\begin{aligned}&\Delta C_1(j\omega)\\&= \left[k_{i11}\, N_e\left(-\omega^2\right) - k_{p11}\omega^2\, N_0\left(-\omega^2\right) - \omega^2 D_0\left(-\omega^2\right)\right]\\&= +j\left[k_{p11}\omega N_e\left(-\omega^2\right) + k_{il1}\omega N_0\left(-\omega^2\right) + \omega D_e\left(-\omega^2\right)\right]\end{aligned} \tag{51}$$

Equating the real and imaginary components $\Delta C_1(j\omega)$ to zero, one can derive equation (50).

$$\begin{aligned}k_{i11}N_e\left(-\omega^2\right) - k_{p11}\omega^2 N_0\left(-\omega^2\right) &= \omega^2 D_0\left(-\omega^2\right)\\k_{p11}\omega N_e\left(-\omega^2\right) + k_{i11}\omega N_0\left(-\omega^2\right) &= -\omega\, D_e\left(-\omega^2\right)\Big]\end{aligned} \tag{52}$$

Solving (52), ranges of stability k_{p11}(0-0.22) and k_{i11} (0-0.077) were obtained.

The same methods were used to get the matching tuning gains for the reactive torque and flux loops.

$$G_r(s) = \frac{G_{c3}(s)T_v}{sT_m + G_{c3}(s)T_m} = \frac{k_{p22}s + k_{i22}}{s^2 + (0.775 + k_{p22})s + k_{i22}} \tag{53}$$

The reactive torque loop has the same TF, as electromagnetic torque and the same gains can be considered.

Representing flux loop (w21) open loop TF without $G_{c4}(s)$ as,

$$G_{o2}(s) = G_r(s)G_s(s) = \frac{0.84s + 3.37}{s^3 + 7.03s^2 + 25.24s + 0.85} \tag{54}$$

Ranges of stability kp_{22}(3-8) and ki_{22} (0.12-0.55) were obtained by applying equations from (50)–(52).

Despite the fact that Gc3(s)-1 has large overshoot, still it is stable but very close to unstable region than the other two controllers shown by figure 8 (a) as can be seen from the data in Table 2. The closed-loop unit step responses in Figures 8 (a) and (b), Gc3(s)-2 is less stable than Gc3(s)-3. In the case of Gc4(s) dropping from Gc4(s)-3 is unstable and Gc4(s)-1 is more stable than Gc4(s)-2.

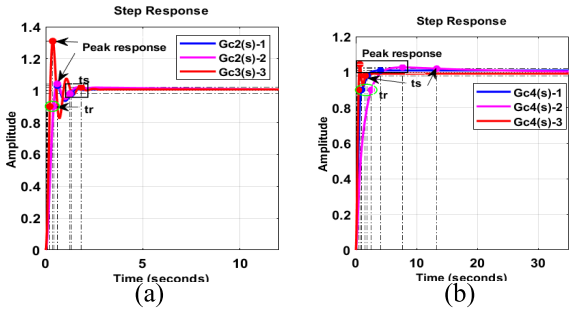

FIGURE 8. (a) speed and (b) flux loops step response.

The following conclusion can be drawn from Table 3's analysis of the relationship between phase margin (Pm) and gain margin (Gm).

TABLE 2. PI design parameters and performance values.

Performance values	Gc2(s)			Gc4(s)		
	1	2	3	1	2	3
k_p	0.2	0.1	0.5	14	6	25
K_i	0.02	0.02	0.05	0.8	0.4	0.1
$t_s(s)$	1.4	1.42	1.85	2.4	14	2
$t_r(s)$	0.43	0.45	0.2	0.15	0.3	0.1
$M_p\%$	0.18	0.2	0.35	0.01	0.03	0.08

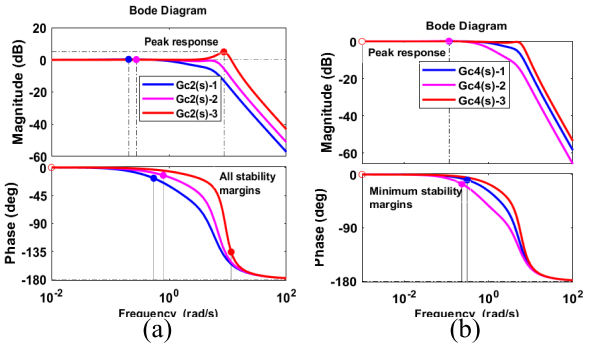

FIGURE 9. Bode plot of (a) speed and (b) flux control loops.

If both the Gm and the Pm are positive, the control system is stable; if one or both of them are negative, the control system is unstable. Marginally stable conditions occur when the Gm and the Pm are equal to zero.

TABLE 3. PI design parameters and performance values.

Performance values	Gc2(s)			Gc4(s)		
	1	2	3	1	2	3
Gm	∞	∞	∞	∞	∞	∞
Pm(deg)	163	154	44.3	171	164	-180
Stable?	yes	yes	yes	yes	yes	no

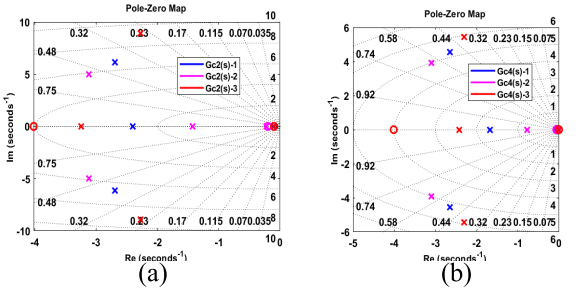

FIGURE 10. Pole-zero map of the (a) speed closed-loop and (b) flux closed: zeros are determined by circles, while poles by crosses.

C. EXPERIMENTAL RESULTS

The experiment involved a 5.5 kW drive system driven by a voltage source converter (VSC). Table 4 lists the electric driving system's parameters. The control system was built with a

DSP Sharc ADSP21363 floating-point signal processor and an Altera Cyclone 2 FPGA.

TABLE 4. IM parameters and references unit.

Quantity	Symbol	Values (p.u)
Stator, rotor resistances	*Rs, Rr*	0.025, 0.068
Core resistance	*Rcb*	15
Magnetizing inductance	*Lm*	3.98
Stator, rotor inductances	*Ls,Lr*	4.07
Leakage inductance	*Lls*	0.017H
Nominal Power	*Pn*	5.5 kW
Nominal stator current, voltage	*In, Un*	11 A, 400V
Nominal rotor speed	*n*	14300 rpm
Nominal frequency	*f*	500 Hz
Reference current	$Ib = In\sqrt{3}$	19 A
Reference voltage	*Ub=Un*	400 V
Reference power	*Pb*	7.6 kW

Implementing the loss minimization model, the induction motor should be managed so that the necessary air gap is maintained at the necessary level, as far away from the stator frequency or stator current as is practicable. It is advised to maintain the airgap flux at its rated value for the quick drive response to reduce the time required for torque buildup.

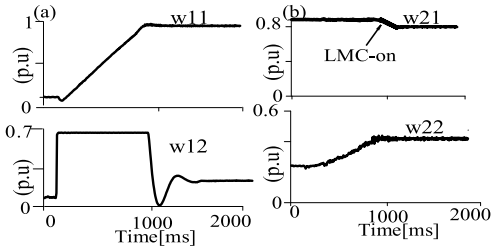

FIGURE 11. (a) Unloaded IM is starting up to 1 (w11) electromagnetic torque (w12) and (b) square of rotor flux (w21), reactive torque (w22) using proposal 1.

The results for the model that accounts for core loss in Figure 12 demonstrate a faster (a) speed reversal to −1 p.u with electro mechanical torque and (b) comparison of un optimized and optimized flux, reactive torque.

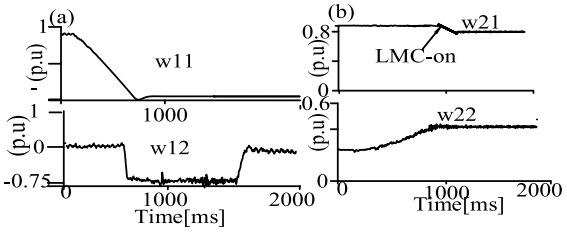

FIGURE 12. IM is reversing to −1 (w11), (w12) and (b) square of rotor flux (w21), reactive torque (w22) using proposal 1.

Figure 13 depicts (a) the reference speed, estimated speed, optimum loss minimizing flux starting up 1 p.u and (b) electromagnetic torque for the load torque of 0.5p.u.

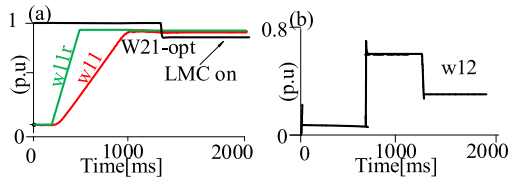

FIGURE 13. Speed (w11), reference speed (w11r) and optimum flux (w21_optimum) when LMC is applied and (b) electromagnetic torque for the load torque of 0.5p.u using proposal.

Figure 14(a) below shows the results obtained when loss minimization is omitted vs the optimal flux level. Nevertheless, the disregard for loss-minimizing control (LMC) results in a larger flux demand than consideration of LMC. Unnecessary current increases due to the excess flux, increasing the power wasted in the copper and core. The core loss rises with speed, as seen in Figure 16(b) below. Core loss decreased significantly from 0.03 p.u. (165 W) to 0.025 p.u. (0.138 kW).

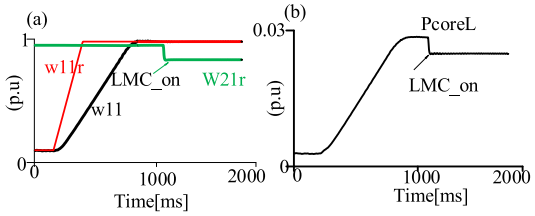

FIGURE 14. (a) Reference speed (w11r), speed (w11), reference flux (w21r) and (b) core loss (PcoreL) under proposal 1.

In Figure 15 (a), the rotor copper loss is around 0.015 p.u. (0.83kW), and the stator copper loss is 0.02 p.u. (0.11kW) when LMC applied. Figure 9 (b) below shows the total loss is 0.06 p.u. (0.33kW). Evidence suggests that implementing LMC leads to a notable decrease in the machine's overall losses, hence improving energy efficiency.

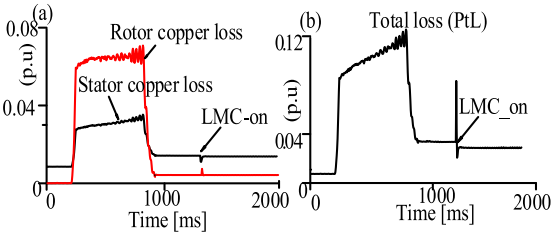

FIGURE 15. Measured (a) rotor (PrCuL) and stator (PsCuL) and (b) total (PtL) losse under proposal 1.

Figure 16 below shows the experimental result obtained when the optimization technique proposed from the idea of magnetizing nature of the variable w22 having meaning full impact on loss of machine. It can be seen from the result that more reduction in flux than using proposal 1 without affecting the performance of the control system at all.

In Figure 21 shows the stator 0.017p.u (0.965kW) and rotor 0.013p.u (0.715kW) and core loss of 0.018p.u (0.984kW) under proposal 2.

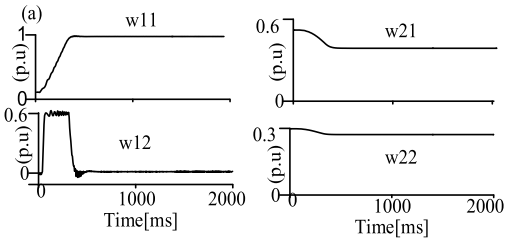

FIGURE 16. (a) Unloaded IM is starting up to 1 (w11) electromagnetic torque (w12) and (b) square of rotor flux (w21), reactive torque (w22) using proposal 2.

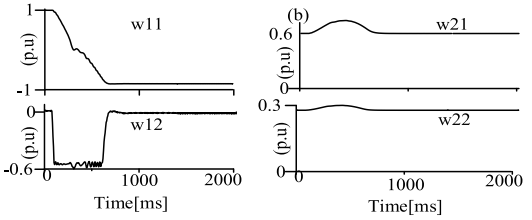

FIGURE 17. IM is reversing to −1 (w11), (w12) and (b) square of rotor flux (w21), reactive torque (w22) using proposal 1.

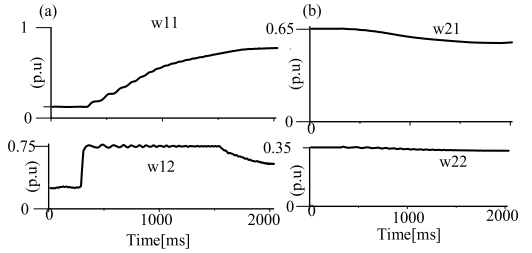

FIGURE 18. (a) Speed, electromagnetic torque and (b) flux, reactive torque when machine loaded about $TL = 0.5$ p.u using proposal 2.

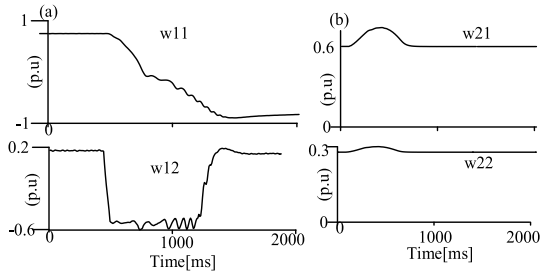

FIGURE 19. (a) Speed reversal, electromagnetic torque and (b) flux, reactive torque machine loaded about $TL = 0.4$ p.u using proposal 2.

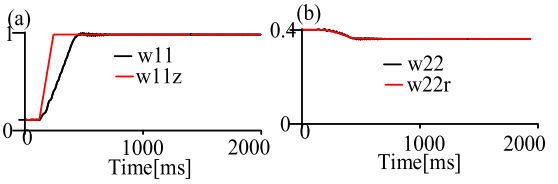

FIGURE 20. (a) Reference speed (w11r), speed (w11), and (b) reference reactive torque (w22r) and reactive torque (w22) under proposal 2.

Figure 22 below shows the rotor (PrCuL) about 0.036p.u (0.98kW), stator (PsCuL) about 0.042p.u (0.231kW)cupper losses are dependent on the load torque resulting in an increase of the total machine loss and the core loss is independent of the load torque.

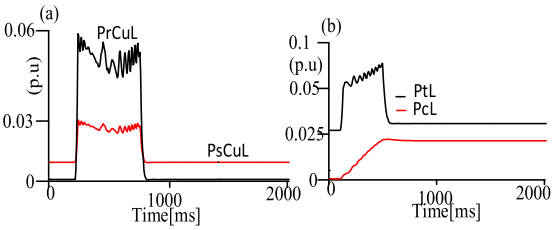

FIGURE 21. Measured (a) rotor (PrCuL) and stator (PsCuL) copper losses and (b) total (PtL) and core (PcL) losses under proposal 2.

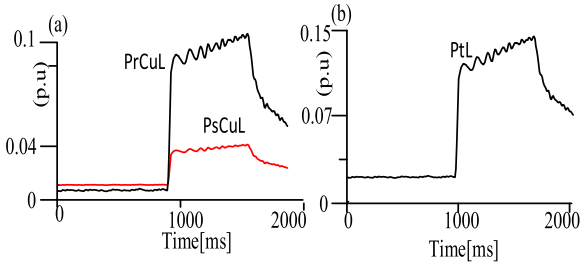

FIGURE 22. Measured (a) rotor (PrCuL) and stator (PsCuL) and (b) total (PtL) loss when machine loaded about $TL = 0.4$ under proposal 2.

TABLE 5. Comparison of the proposed optimizations.

Losses (W)	Proposal 1	Proposal 2
Copper losses	192.5	168
Core loss	137.5	98.4
Total loss	330	266.4

In the context of model-based analysis and design, the accuracy of the model parameters significantly impacts the outcomes.

Figure 23 below shows the uncertainties of parameters of HSIM. The observer structure's response to variations in the stator and rotor resistance in this case. During these testing, the AFO speed estimation scheme was applied. IM loads at around TL = 0.5 p.u. After 10s, the rotor resistance in Fig. 23(a) changes (Rr = 1.75RrN). The uncertainty in rotor speed estimation rises to around 0.012–0.017 p.u. The rotor resistance value has a significant impact on the AFO structure errors. The stator resistance in Fig. 23(b) is adjusted from 0.025 to 0.045 p.u. (Rs = 1.75RsN). Up to roughly 0.02 p.u., the rotor speed estimation inaccuracy rises.

The results show that core resistance and speed mainly influences core loss, Rs, Lm and TL mainly affects copper loss. As the parameter error rises, these impacts get stronger. Rr, Ls and Lr has little to no impact on copper and core loss.

Figures 24 and 25 depicts laboratory setup and the entire sensorless control system respectively.

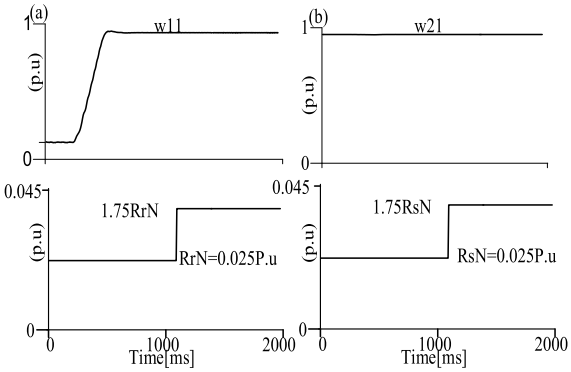

FIGURE 23. After 1000 ms the nominal value of rotor and stator resistances were changed up to 0.045 p.u., the rotor speed is reproduced adaptively, the machine is loaded about 0.5 p.u.

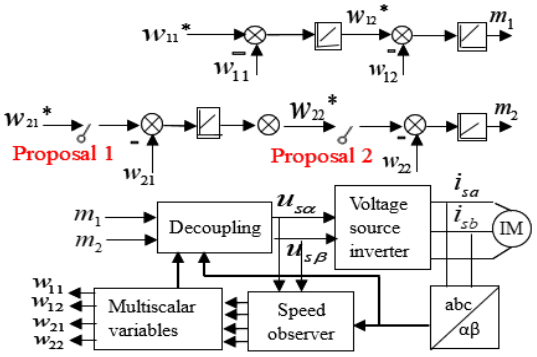

FIGURE 24. Sensorless control system scheme.

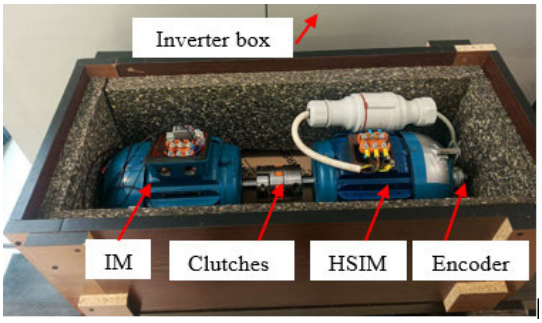

FIGURE 25. Experimental stand with HSIM coupled to IM.

VI. CONCLUSION

A sensorless speed control of HSIM with optimum flux and reference reactive torque based optimization techniques were proposed for loss minimization. The reference reactive torque based proposed optimization was robust specially in dynamic state reducing the loss components more with less PI controllers omitting flux controller and hence less tunings. The measured core loss without considering optimization technique was 165W with percentage reduction in core loss to 16.66% and 26.54% using proposal 1 and proposal 2 respectively.

REFERENCES

[1] D. Sobczyński, "Review of solutions used in high speed induction motor drives operating in household appliances," *Power Electron. Drives*, vol. 1, no. 36, pp. 27–39, 2016, doi: 10.5277/PED160102.

[2] J. Klíma, M. Mach, and O. Vítek, "Analysis of high speed squirrel cage induction motors," in *Proc. IEEE 15th Int. Conf. Environ. Electr. Eng. (EEEIC)*, Rome, Italy, Jun. 2015, pp. 1302–1305, doi: 10.1109/EEEIC.2015.7165358.

[3] J. F. Gieras and J. Saari, "Performance calculation for a high-speed solid-rotor induction motor," *IEEE Trans. Ind. Electron.*, vol. 59, no. 6, pp. 2689–2700, Jun. 2012, doi: 10.1109/TIE.2011.2160516.

[4] W. L. Soong, G. B. Kliman, R. N. Johnson, R. A. White, and J. E. Miller, "Novel high-speed induction motor for a commercial centrifugal compressor," *IEEE Trans. Ind. Appl.*, vol. 36, no. 3, pp. 706–713, Jun. 2000, doi: 10.1109/28.845043.

[5] J. Pyrhonen, J. Nerg, P. Kurronen, and U. Lauber, "High-speed high-output solid-rotor induction-motor technology for gas compression," *IEEE Trans. Ind. Electron.*, vol. 57, no. 1, pp. 272–280, Jan. 2010, doi: 10.1109/TIE.2009.2021595.

[6] P. R. Matić, A. Ž. Rakić, D. P. Marčetić, and S. N. Vukosavić, "Improved torque control of high speed shaft-sensorless induction motor drive," *Automatika*, vol. 56, no. 4, pp. 443–453, Jan. 2015, doi: 10.1080/00051144.2015.11828658.

[7] P. Stopa and K. Lu, "High speed field oriented control," M.S. thesis, IET, AAU, Esbjerg, Copenhagen, Jun. 2009. [Online]. Available: https://projekter.aau.dk/projekter/files/17642794/out.html

[8] W. Choi, S. Li, and B. Sarlioglu, "Core loss estimation of high speed electric machines: An assessment," in *Proc. IECON*, Vienna, Austria, Nov. 2013, pp. 2691–2696, doi: 10.1109/IECON.2013.6699556.

[9] J. Lahteenmaki, "Design and voltage supply of high-speed induction machines," Ph.D. thesis, Dept. Elect. Commun. Eng., Helsinki Univ. Technol., Espoo, Finland, 2002, pp. 1–140.

[10] T. Jokinen, "Losses of high-speed induction motors," *Prace Instytutu Elektrotechniki*, vol. 223, pp. 71–79, Jan. 2005.

[11] J. Saari, "Thermal modelling of high-speed induction machines," in *Acta Polytechnica Scandinavica* (Electrical Engineering Series), no. 82. Helsinki, Finland: Finnish Academy of Technical Sciences, 1995, pp. 1–82.

[12] K. Jalili, D. Krug, S. Bernet, M. Malinowski, and B. J. C. Filho, "Design and characteristics of a rotor flux controlled high speed induction motor drive applying two-level and three-level NPC voltage source converters," in *Proc. IEEE 36th Power Electron. Spec. Conf.*, Jun. 2005, pp. 1820–1826, doi: 10.1109/PESC.2005.1581878.

[13] A. Boglietti, P. Ferraris, M. Lazzari, and M. Pastorelli, "Influence of the inverter characteristics on the iron losses in PWM inverter-fed induction motors," *IEEE Trans. Ind. Appl.*, vol. 32, no. 5, pp. 1190–1194, Sep. 1996, doi: 10.1109/28.536882.

[14] W.-C. Tsai, "Effect of inverter parameters on iron losses in a PWM inverter-fed induction motor," in *Proc. 4th Int. Conf. Innov. Comput., Inf. Control (ICICIC)*, Kaohsiung, Taiwan, Dec. 2009, pp. 914–917, doi: 10.1109/icicic.2009.188.

[15] A. Boglietti, P. Ferraris, M. Lazzari, and F. Profumo, "Effects of different modulation index on the iron losses in soft magnetic materials supplied by PWM inverter," *IEEE Trans. Magn.*, vol. 29, no. 6, pp. 3234–3236, Nov. 1993, doi: 10.1109/20.281147.

[16] A. Boglietti, "PWM inverter fed induction motors losses evaluation," *Electr. Mach. Power Syst.*, vol. 22, no. 3, pp. 439–449, May 1994, doi: 10.1080/07313569408955578.

[17] M. C. Di Piazza and M. Pucci, "Efficiency issues in induction motor drives: Modelling and losses minimization techniques," in *Proc. IEEE Workshop Electr. Mach. Design, Control Diagnosis (WEMDCD)*, Turin, Italy, Mar. 2015, pp. 171–177, doi: 10.1109/WEMDCD.2015.7194526.

[18] A. Boglietti, P. Ferraris, M. Lazzari, and M. Pastorelli, "Change of the iron losses with the switching supply frequency in soft magnetic materials supplied by PWM inverter," *IEEE Trans. Magn.*, vol. 31, no. 6, pp. 4250–4252, Nov. 1995, doi: 10.1109/20.489942.

[19] E. N. Hildebrand and H. Roehrdanz, "Losses in three-phase induction machines fed by PWM converter," *IEEE Trans. Energy Convers.*, vol. 16, no. 3, pp. 228–233, Sep. 2001, doi: 10.1109/60.937201.

[20] M. Ikeda, S. Sakabe, and K. Higashi, "Experimental study of high speed induction motor varying rotor core construction," *IEEE Trans. Energy Convers.*, vol. 5, no. 1, pp. 98–103, Mar. 1990, doi: 10.1109/60.50819.

[21] C. Kim, K.-S. Lee, and S.-J. Yook, "Effect of air-gap fans on cooling of windings in a large-capacity, high-speed induction motor," *Appl. Thermal Eng.*, vol. 100, pp. 658–667, May 2016, doi: 10.1016/j.applthermaleng.2016.02.077.

[22] S. Li, Y. Li, W. Choi, and B. Sarlioglu, "High-speed electric machines: Challenges and design considerations," *IEEE Trans. Transport. Electrific.*, vol. 2, no. 1, pp. 2–13, Mar. 2016, doi: 10.1109/TTE.2016.2523879.

[23] K. Aiso and K. Akatsu, "Performance comparison of high-speed motors for electric vehicle," *World Electr. Vehicle J.*, vol. 13, no. 4, p. 57, Mar. 2022, doi: 10.3390/wevj13040057.

[24] J. Pyrhonen, "Calculating the effects of solid-rotor material on high-speed induction motor characteristics," *Eur. Trans. Electr. Power*, vol. 1, no. 6, pp. 301–310, Nov. 1991, doi: 10.1002/etep.4450010602.

[25] W. Chou, Y. Liang, L. Gao, and D. Wang, "Research on eddy current losses algorithm in solid rotor of high speed squirrel cage induction motor," *IET Electr. Power Appl.*, vol. 14, no. 6, pp. 1023–1029, Mar. 2020, doi: 10.1049/iet-epa.2019.0884.

[26] M. O. Gulbahce and D. A. Kocabas, "High-speed solid rotor induction motor design with improved efficiency and decreased harmonic effect," *IET Electr. Power Appl.*, vol. 12, no. 8, pp. 1126–1133, Jan. 2018, doi: 10.1049/iet-epa.2017.0675.

[27] B.-H. Bae, S.-K. Sul, J.-H. Kwon, and J.-S. Byeon, "Implementation of sensorless vector control for super-high-speed PMSM of turbo-compressor," *IEEE Trans. Ind. Appl.*, vol. 39, no. 3, pp. 811–818, May 2003, doi: 10.1109/TIA.2003.810658.

[28] K. L. Shi, T. F. Chan, Y. K. Wong, and S. L. Ho, "Speed estimation of an induction motor drive using an optimized extended Kalman filter," *IEEE Trans. Ind. Electron.*, vol. 49, no. 1, pp. 124–133, Feb. 2002, doi: 10.1109/41.982256.

[29] M. Comanescu, "Design and implementation of a highly robust sensorless sliding mode observer for the flux magnitude of the induction motor," *IEEE Trans. Energy Convers.*, vol. 31, no. 2, pp. 649–657, Jun. 2016, doi: 10.1109/TEC.2016.2516951.

[30] M. Morawiec, "Z-type observer backstepping for induction machines," *IEEE Trans. Ind. Electron.*, vol. 62, no. 4, pp. 2090–2102, Apr. 2015, doi: 10.1109/TIE.2014.2355417.

[31] M. Morawiec, P. Kroplewski, and C. Odeh, "Nonadaptive rotor speed estimation of induction machine in an adaptive full-order observer," *IEEE Trans. Ind. Electron.*, vol. 69, no. 3, pp. 2333–2344, Mar. 2022, doi: 10.1109/TIE.2021.3066919.

[32] D. P. Marcetic, I. R. Krcmar, M. A. Gecic, and P. R. Matic, "Discrete rotor flux and speed estimators for high-speed shaft-sensorless IM drives," *IEEE Trans. Ind. Electron.*, vol. 61, no. 6, pp. 3099–3108, Jun. 2014, doi: 10.1109/TIE.2013.2258311.

[33] B. Park, D. Kim, P. Han, Y. Chun, and J. Choi, "Sensorless control using improved stator flux estimator for high-speed induction motors," in *Proc. ICEMS*, Pattaya, Thailand, Oct. 2015, pp. 116–121, doi: 10.1109/ICEMS.2015.7385010.

[34] Y. Han, Z. Nie, J. Xu, J. Zhu, and J. Sun, "Control strategy for optimising the thrust of a high-speed six-phase linear induction motor," *IET Power Electron.*, vol. 13, no. 11, pp. 2260–2268, Jun. 2020, doi: 10.1049/iet-pel.2019.1334.

[35] R. Goleman, "A high-speed induction motor making use of the third harmonic of the magnetic flux," *J. Magn. Magn. Mater.*, vol. 133, nos. 1–3, pp. 624–626, May 1994, doi: 10.1016/0304-8853(94)90639-4.

[36] P. Ferraris, M. Lazzari, and F. Villata, "High-speed induction motor drives: Starting operation control," *IFAC Proc.*, vol. 16, no. 16, pp. 353–359, Sep. 1983, doi: 10.1016/S1474-6670(17)61889-5.

[37] Z. Krzeminski, "Nonlinear control of induction machines," *Proc. 10th IFSC World Congr.*, Munich, Germany, 1987, pp. 349–354.

[38] M. Adamowicz and J. Guzinsk, "Minimum-time minimum-loss speed sensorless control of induction motors under nonlinear control," in *Proc. IEEE Compat. Power Electron.*, Gdynia, Poland, Jun. 2005, pp. 1–7, doi: 10.1109/CPE.2005.1547546.

[39] C. C. de Wit and J. Ramirez, "Optimal torque control for current-fed induction motors," *IEEE Trans. Autom. Control*, vol. 44, no. 5, pp. 1084–1089, May 1999, doi: 10.1109/9.763235.

[40] E. S. Abdin, G. A. Ghoneem, H. M. M. Diab, and S. A. Deraz, "Efficiency optimization of a vector controlled induction motor drive using an artificial neural network," in *Proc. IECON 29th Annu. Conf. IEEE Ind. Electron. Soc.*, vol. 3, Roanoke, VA, USA, Jun. 2003, pp. 2543–2548, doi: 10.1109/IECON.2003.1280646.

[41] J.-F. Stumper, A. Dötlinger, and R. Kennel, "Loss minimization of induction machines in dynamic operation," *IEEE Trans. Energy Convers.*, vol. 28, no. 3, pp. 726–735, Sep. 2013, doi: 10.1109/TEC.2013.2262048.

[42] T. Ayana, M. Morawiec, and L. Wogi, "Multiscalar control based airgap flux optimization of induction motor for loss minimization," *IEEE Access*, vol. 12, pp. 19993–20002, 2024, doi: 10.1109/ACCESS.2024.3359176.

[43] A. Yuce, "Analytical design of PI controller for first order transfer function plus time delay: Stability triangle approach," *IEEE Access*, vol. 11, pp. 70377–70386, 2023, doi: 10.1109/ACCESS.2023.3292830.

TADELE AYANA received the B.Sc. degree in electrical and computer engineering from Jimma University, in 2013, and the M.Sc. degree in control and instrumentation engineering from the Jimma Institute of Technology, Jimma, Ethiopia, in 2018. He is currently pursuing the Ph.D. degree with the Faculty of Electrical and control Engineering, Department of Electric Drives and Energy Conversion, Gdańsk University of Technology, Gdańsk, Poland. Since 2018, he has been a Lecturer with the Jimma Institute of Technology. He is the author of more than seven articles. His main research interests include multiscalar models, nonlinear control of electrical machines, sensorless control, nonlinear control, adaptive observer, and sliding mode control.

PIOTR KOŁODZIEJEK received the Ph.D. degree from Gdańsk University of Technology, Gdańsk, Poland. Since 2010, he has been an Assistant Professor with Gdańsk University of Technology. His research interests include the control and diagnosis of electrical machines, renewable energy sources, and energy storage systems.

MARCIN MORAWIEC (Senior Member, IEEE) received the M.Sc. degree in electrical engineering from Częstochowa University of Technology, Poland, in 2003, the Ph.D. degree from Gdańsk University of Technology, Gdańsk, Poland, in 2007, and the D.Sc. degree in electrical drives, in 2017. He is currently a Professor with Gdańsk University of Technology. He is the author of more than 70 articles and two monographs and two chapters in books, one Polish patent, and five patent applications. His main research interests include multiscalar models, nonlinear control of any electrical machine, sensorless control, nonlinear control, backstepping control, adaptive observer backstepping, and sliding mode control.

LELISA WOGI received the B.Sc. degree in electrical and computer engineering from Jimma University, in 2017, and the M.Sc. degree in control and instrumentation engineering from Jimma Institute of Technology, Jimma, Ethiopia, in 2022. He is currently pursuing the Ph.D. degree with the Faculty of Electrical and Control Engineering, Department of Electric Drives and Energy Conversion, Gdańsk University of Technology, Gdańsk, Poland. Since 2017, he has been an Assistant Lecturer with Bule Hora University. He is the author of more than five articles. His main research interests include nonlinear control of electrical machines, sensorless control, nonlinear control, adaptive observer, and sliding mode control.